

# COMPARATIVE STUDY OF TWO TYPES OF MEDIUM TEMPERATURE PHASE CHANGE MATERIALS

SOL-CAROLINA COSTA<sup>1</sup>, MOHAMMAD ISMAIL<sup>1</sup>, MURAT KENISARIN<sup>1</sup>,  
 KHAMID MAHKAMOV<sup>1</sup>, DAVID MULLEN<sup>2</sup>, ELVEDIN HALIMIC<sup>2</sup> & KEVIN LYNN<sup>2</sup>  
<sup>1</sup>Northumbria University, UK  
<sup>2</sup>Aavid Thermacore, UK

## ABSTRACT

This work presents a numerical comparative study of the melting and solidification processes of two medium temperature phase change materials (PCMs) for latent heat thermal energy storage (LHTES) applications. The PCMs compared are an inorganic solar salt and a Sn-based metal alloy, with the phase change temperatures around 220°C. The numerical comparative study was conducted in a 2D rectangular unit model with constant heat flux, the simulations were conducted deploying the enthalpy method in Ansys FLUENT software. The numerical results were validated using experimental results for one of the phase change materials studied. The charging and discharging times of the designed LHTES were studied for both phase change materials, finding that the metallic PCM LHTES showing superior performance. The charging and discharging time obtained for the solar salt LHTES, duplicate the time required using metallic PCM LHTES. Moreover, the final average temperature for the solar salt LHTES, shows significantly compare with the phase change temperature.

*Keywords: PCM, LHTES, melting, solidification, metallic PCM, thermal properties.*

## 1 INTRODUCTION

For several decades, latent thermal energy storage systems (LHTES) have been successfully used in numerous engineering applications such as solar plants, thermal management solutions, etc. In general, the phase change materials (PCMs) have a high energy storage density and small temperature variation during LHTES charging and discharging periods. The main disadvantage of currently used PCMs (organic materials and hydrated salts) is the low thermal conductivity which limits their application for processes that need high heat transfer rates. Therefore, it is necessary to deploy methods, which would enhance the heat transfer in the LHTES. There are several techniques used to enhance the heat transfer in the LHTES and these include adding high thermal conductive particles or placing high thermal conductivity insertions, such as metallic fins or porous matrices [1]. The performances of finned heat pipes coupled to different PCMs for cooling of electronic devices were experimentally and numerically studied in [2]. Metallic PCMs (MPCMs) were first considered for thermal storage more than four decades ago [3], however, due to mainly excessive weight and cost, compared to organics and salt hydrate PCMs, these were not used in LHTES applications and there is a very limited number of studies in this area. Disadvantages, related to the excessive weight, are partially compensated by the high thermal conductivity of appropriate metallic materials and the high thermal capacity of LHTES per unit of volume. The feasibility of application of MPCMs improves with the cost reduction of metallic materials using low purity alloys.

The aim of this work is to compare numerically the melting and solidification processes in two small physical models of medium temperature LHTES with solar salt and MPCM. The melting processes are studied in a rectangular shaped LHTES cells with the application of constant heat flux, provided by cylindrical heating cartridges, placed in the cells.



## 2 MEDIUM TEMPERATURE PHASE CHANGE MATERIALS

The LHTES cells for experimental tests were developed with a thermal storage capacity of about 1 kWh to model medium temperature solar thermal storage applications at temperature levels of about 220°C. The thermal energy accumulated in a larger scale LHTES can be used, for example, to extend the operational period of an organic Rankine cycle (ORC) turbine [4] or other converters in solar thermal electricity plants [5].

Fig. 1 presents results from literature review of information on PCMs to be used in the temperature range from 300 to 1,200 K with indication of their costs per kWh [5]. In the medium temperature range (about 220°C) mainly salts and metals make up a significant fraction of available PCMs. However, only for a few of them the complete set of thermal properties is available in the literature [6]. Among materials, solar salt (60 wt.% NaNO<sub>3</sub>+40 wt.% KNO<sub>3</sub>) and the equimolar eutectic blend (46.7 wt.% NaNO<sub>3</sub>+40 wt.% KNO<sub>3</sub>) are those which were extensively investigated [7]. Also, tin and its alloys can be used as a PCM in special cases, in which the weight and cost are not critical factors for an application.

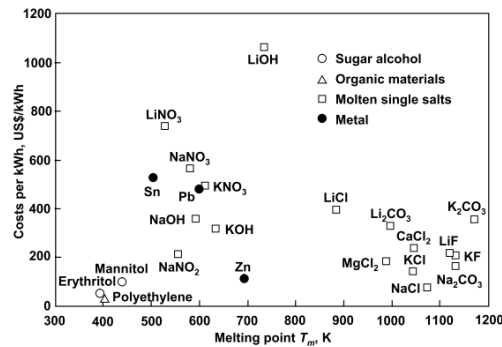


Figure 1: Media costs of PCMs [5].

In the temperature range studied, the preferable candidates are solar salt and tin based alloys (see Table 1). In this work, efforts were concentrated on obtaining the thermo-physical properties of three metallic PCMs, including their phase transition temperature, the heat of fusion and the specific heat.

Fig. 1 shows the costs per kWh for different PCMs and around the 500 K temperature level application Sn, pure nitrate salts KNO<sub>3</sub> and NaNO<sub>3</sub> have similar values. In 2005 the price of pure tin was lower than 10.000 US\$/tonne. The price for pure tin has increased in the last years; however, the price depends on its purity grade and in certain cases the price difference between high and low purity materials is significant. When evaluating the cost of PCM/additive composition it is vital to include the cost of additives, used to enhance the thermal conductivity of composite, since quite often the cost of additives per unit of mass are significantly higher than that for pure PCMs.

### 2.1 Thermo-physical properties of the selected PCMs

The melting temperature, the heat of fusion and the specific heat capacity were determined for solar salt, Sn, 96.5Sn-3.5Ag (wt.%) and 99.3Sn-0.7Cu (wt.%) using Differential Scanning Calorimeter (DSC) Setaram EVO-131. The results of the DSC carried out in the present work are shown in Fig. 2.

Table 1: Physical properties of PCM candidates.

Wt.%	60 wt.% NaNO <sub>3</sub> +40 wt.% KNO <sub>3</sub>	Tin (Sn)	96.5Sn-3.5Ag	99.3Sn-0.7Cu
H <sub>m</sub> (kJ/kg)	91.5 [8]	64.0 (PW)	62.3 (PW)	64.5 (PW)
T <sub>solidus, m</sub> (°C)	218.9 [8]	232.2 (PW)	221.4 (PW)	226.8 (PW)
T <sub>liquidus, m</sub> (°C)	<b>225.0 [8]</b>	<b>237.2 (PW)</b>	<b>227.7 (PW)</b>	<b>232.9 (PW)</b>
H <sub>s</sub> (kJ/kg)	87.7 [8]	60.7 (PW)	62.3 (PW)	64.6 (PW)
T <sub>solidus, s</sub> (°C)	212.4 [8]	170.6 (PW)	214.6 (PW)	201.2 (PW)
T <sub>liquidus, s</sub> (°C)	218.5 [8]	173.0 (PW)	212.4 (PW)	–
ρ <sub>l</sub> (kg/m <sup>3</sup> )	1,958 [9]	6974 [10]	6,998 [11]	7,067 [12]
β (1/K)	3.47E-04 [9]	1.14E-04 [10]	9.55E-05 [11]	1.13E-04 [12]
k (W/m K)	0.380 [9]	73(s) [6]	84 (s) [13]	58.9 (s) 44.8 (l) [14]
C <sub>p</sub> (J/kg.K)	1620 [9]	222 [6]	260 [15]	220 [6]

PW = present work.

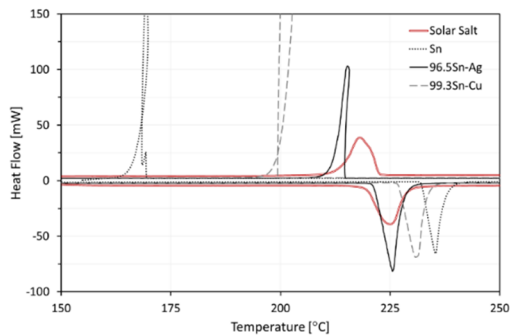


Figure 2: The typical DSC analysis for the PCMs.

It can be observed that the melting temperatures are between 225 and 237°C for these PCMs. However, during the solidification process of pure tin, a high degree of supercooling (approximated 50°C) is observed during the transformation from the liquid to solid state. The supercooling is clearly reduced for the Sn-based alloys, however, the alloy which has the phase transition temperatures closer to that of solar salt is 96.5Sn-3.5Ag (wt.%). In general, the thermal hysteresis can be observed during phase change in PCMs.

Table 1 summarizes the results obtained for metallic PCMs and solar salt. Each value is obtained as the average value of three measurements. This data obtained from DSC tests is used in the process of designing and numerical simulations of operation of the LHTES cells. For simulation purposes, data on the density, thermal conductivity and viscosity were obtained from other references.

When comparing the thermophysical properties, the main advantage of solar salt can be seen, which is the high heat of fusion. Its main drawback is the low thermal conductivity. The metallic PCMs have much higher values of the thermal conductivity but the heat of fusion per unit of mass is relatively small, resulting in the excessive mass of the LHTES.

## 2.2 The LHTES cell design

The LHTES cell is designed in order to provide thermal energy at the rate of 0.25 kW for the duration of 4-hour period [4]. In order to store this amount of the thermal energy as a latent heat, about 39 kg of solar salt or 58 kg of the metal alloy are necessary. The charging of the cell is carried out by applying a constant heat flux produced by cylindrical cartridges placed in the cell, this mean that the heat transfer rate to the LHTES is fixed. These cartridges simulate the charging process by heat pipes [4]. The number of heat pipes installed in the cell is two with the maximum heating/cooling rate of 125 W each with a length of 500 mm.

Table 2 shows the LHTES cells characteristics in terms of weight and volume. The mass of the PCM is increased by a factor of 1.5 using metallic PCMs and the volume is decreased by 60%. The volume of the solar salt LHTES cell is 0.020 m<sup>3</sup>.

Table 2: LHTES cell characteristics.

PCM	Storage capacity energy (kWh)	Mass (kg)	Volume (m <sup>3</sup> )
60 wt.% NaNO <sub>3</sub> +40 wt.% KNO <sub>3</sub>	1	39	0.020
96.5Sn-3.5Ag (wt.%)	1	58	0.008
96.5Sn-3.5Ag (wt.%)	2.5	142	0.020

## 3 NUMERICAL MODELING OF LHTES

The aim of the numerical modelling is to compare the performance of these two different PCMs for application in medium temperature solar LHTES. The numerical modelling uses a 2D simplified representation of a cell considering the heat pipe as a constant heat flux device [16]. The physical geometry of the cell unit with heat pipes embedded is shown in Fig. 3. The width and height of the selected frontal area are 142 and 283 mm, respectively, for the 0.020 m<sup>3</sup> LHTES and 58 and 283 mm, respectively, for the 0.008 m<sup>3</sup> LHTES.

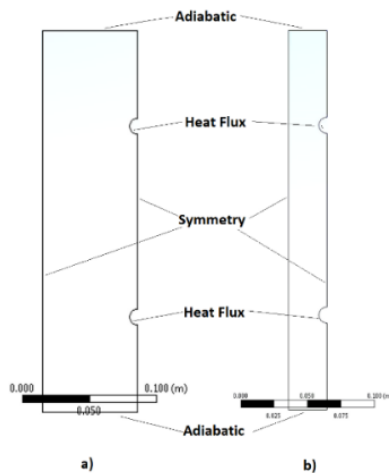


Figure 3: The 2D geometry of the cell. (a) Solar salt (0.020 m<sup>3</sup>); and (b) Metallic (0.008 m<sup>3</sup>).

The commercial software ANSYS Fluent 19.1 was used for simulations of the melting and solidification processes, see Fig. 3. The enthalpy-porosity technique [17]–[19] is deployed to model the PCM melting and solidification processes. In this technique, the mushy zones of PCM are considered as porous media and the porosity of each element in the mushy zone is assumed to be equal to the liquid fraction of that element.

The power law differentiating scheme and SIMPLE method for pressure–velocity coupling are used to solve the momentum and energy conservation equations. The PRESTO scheme is adopted for the pressure correction equation. In the present study, the time step was set to 0.2 s and 0.15 s for the 125 and 250 W of heat transfer rate, respectively. The mesh sensibility analysis is evaluated at 125 W by comparing the variations in liquid fraction and average temperature over three different grid sizes (78,600, 52,400 and 36,800 elements) as is shown in Fig. 4. The results demonstrate that there are not significant differences between the two first grids studied, therefore the computational grid size selected is Mesh 2 (Fig. 4) which has 52,400 elements.

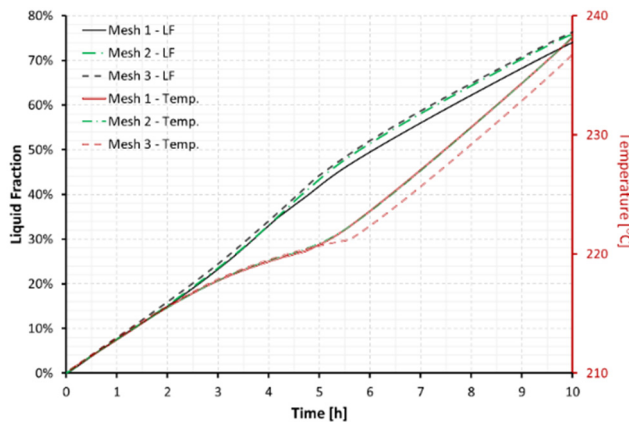


Figure 4: Mesh size sensibility analysis.

The assumptions made in the modelling process are as follows:

- Flow is 2D, laminar and incompressible (no temperature gradient along the LHTES);
- The properties of the PCM are considered constant in both the solid and the liquid phases. The used thermo-physical properties of PCM are listed in Table 1;
- The natural convection effects are modelled by the Boussinesq approximation;
- Thermal expansion is disregarded;
- Constant and uniform heat flux on the surface of heat pipes calculated, considering that the heat transfer rate capacity for both heat pipe is 125 and 250 W;
- Thermal contact resistances are ignored at the interfaces;
- In the cell unit, all vertical walls are symmetry planes and the upper and bottom boundaries are adiabatic walls (Fig. 3).

The numerical model presented in this work for the solar salt was previously experimentally validated using two identical (in the design) prototypes (Fig. 5). The melting and solidification experiments were carried out to validate the numerical melting/solidification models and to study the heat transfer mechanisms in the LHTES [8].





Figure 5: Top view of the container with the PCM [8].

Table 3 shows the experimental and numerical results on determination of the melting and solidification times in both prototypes studied. The liquid fraction, formed in simulations, is also listed for corresponding elapsed times. It can be observed that for the melting process numerical and experimental results agree well with the accuracy within 7%. However, the numerical and experimental results for solidification processes deviate by 18%. The main reason for such the difference is that the solidification process is a free cooling process taking place overnight (governed by the heat losses) and the rate of heat extraction is not controlled during the experiments.

Table 3: Experimental and numerical results [8].

	Melting TC-4 = 225°C	Solidification TC-4 = 212°C
Steel experimental	4.7 h	4.2 h
Steel numerical	4.4 h (LF = 82%)	4.5 h (LF = 11%)
Al. exp.	3.7 h	4.0 h
Al. num.	3.8 h (LF = 97%)	4.8 h (LF = 0%)

### 3.1 Numerical results for charging process

The initial temperature for modelling the charging process is set to 210°C for both PCMs. At this temperature PCMs are in the solid phase at the start of simulations. Fig. 6 shows the evolution of the liquid fraction during the melting process for solar salt and the metallic PCM at heat transfer rate of 125 W. It can be observed that the melting processes of these PCMs are totally different. In the case of solar salt, the buoyancy effect is observed from the start of the melting process. For the metallic PCM, the thermal conduction dominates during all the melting process, which starts much later compared to the case with solar salt. Such behaviour is expected because the Prandtl number of the metallic alloys is close to 0 ( $Pr \ll 1$ ) and therefore the thermal diffusivity dominates, in other words, the heat transfer due to conduction is much greater compared to the convection mechanism. In the case of solar salt, the Prandtl number is approximated 24 ( $Pr \gg 1$ ) therefore the momentum diffusivity dominates and the convection mechanism plays much more intensive role in transferring energy in comparison to pure conduction [20]. In LHTES, where the melting and the solidification of the PCM alternate, the melting process is limited by thermal conductivity and natural convection, and the speed of the solidification process is mainly defined by the thermal conductivity [5].

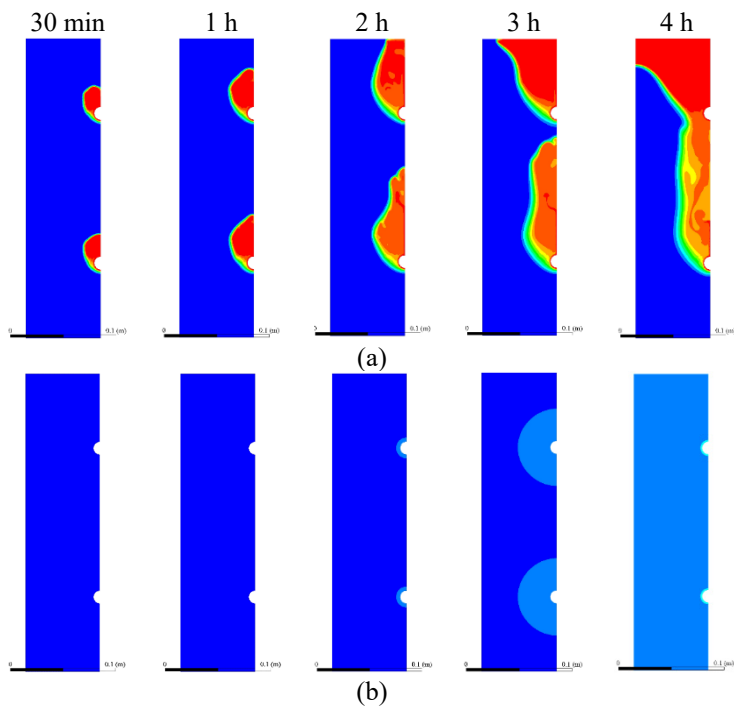


Figure 6: Liquid fraction contours for melting process (125 W) at different elapsed times. (a) Solar salt; and (b) Metallic PCM.

Fig. 7 shows the liquid fraction versus the time during the melting process. In the case of the metallic PCM the melting process is dominated by the thermal diffusivity, therefore the final melting time can be easily calculated (the charging time at the heat transfer rate imposed). Fig. 8 shows the average temperature versus time during the melting process. The phase change during the melting process in the metallic PCM can be divided into three stages: sensible heating of the solid phase, latent heating and sensible heating of the liquid phase. For solar salt, the melting process is dominated by the natural convection at the initial stage and the melting rate is close to that of the metallic PCM for the same storage capacity. After all the material above the heat pipes turn into liquid phase, the melting process rate is drastically reduced, and the thermal diffusivity dominates the melting process. Another important difference is that the temperature in the LHTES with solar salt increases significantly before the melting process is completed (see Fig. 8), therefore the heat thermal storage occurs simultaneously in the form of sensible and latent heat. During the melting process of solar salt, at the initial stage the melting rate is dominated by natural convection therefore, the impact of the heat pipes arrangement is more important than in the case of metallic PCMs. Consequently, the study of the more efficient geometrical shape and heat pipes arrangement is of paramount importance in order to maximize the effect of natural convection.

Table 4 summarises the numerical results on determination of the melting times and average temperature for both types of PCMs studied. The times are the elapsed time from the beginning of the simulation until the liquid fraction makes 90% of the volume. It is observed

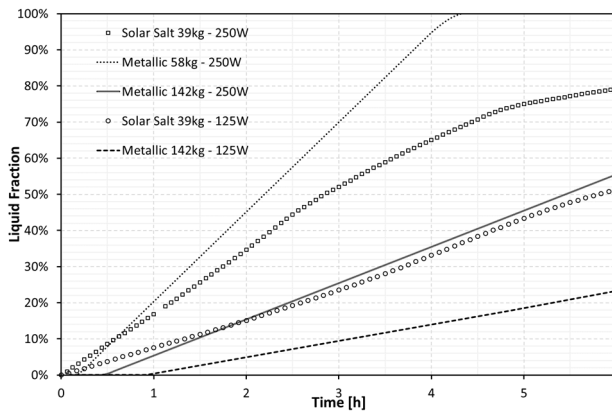


Figure 7: Liquid fraction versus time during melting process.

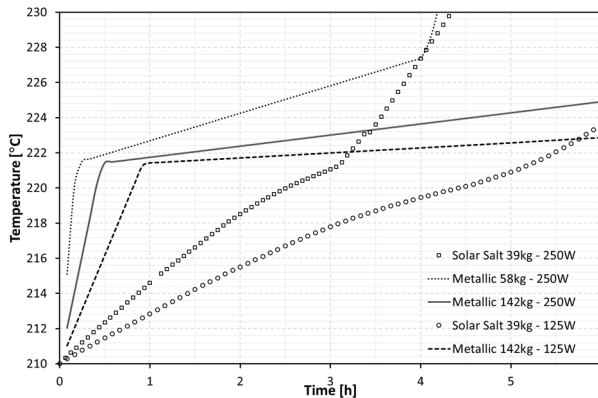


Figure 8: Average temperature versus time during melting process.

that for the metallic PCMs the average temperature in the LHTES is practically the “liquidus” temperature in the different geometries and power supply values studied. However, for solar salt, the temperatures display a significant deviation from the “liquidus” temperature. In Table 4 it can be observed that the metallic LHTES, designed for 1 kWh heat capacity, can be charged in approximated 4 hours (heat transfer rate) and the LHTES with solar salt with the same heat storage capacity require approximately 8 hours. In all the cases the heat transfer rate is controlled but depending on the nature of the heat thermal storage process the melting rate is totally different because the thermal storage process is not purely based on latent heat.

### 3.2 Numerical results for discharging process

The initial temperature for modelling the solidification process is set to the “liquidus” temperature during the melting for solar salt and metallic PCM, which is 225 and 227.7°C, respectively. In the LHTES the initial discharging temperature is determined by a number of

Table 4: Numerical results for melting process (90% liquid fraction).

PCM/LHTES capacity	Total HP power (W)	Melting time (h)	Average temperature (°C)
Solar salt/1kWh	250	~8.0	~270
Metallic/1 kWh	250	3.8	227
Metallic/2.5 kWh	250	9.5	227
Solar salt/1kWh	125	15.7	270
Metallic/2.5 kWh	125	19.5	227

factors: the final charging level, the thermal losses, the characteristic of the PCMs, etc. Fig. 9 shows evolutions of the liquid fraction during the solidification process for solar salt and metallic PCM at heat transfer rate of 125 W. It can be observed that the solidification process for the metallic PCM is practically homogeneous in the whole volume of the LHTES. For solar salt there is a clear stratification process at the beginning and then the solidified material gradually grows circularly around the heat transfer devices.

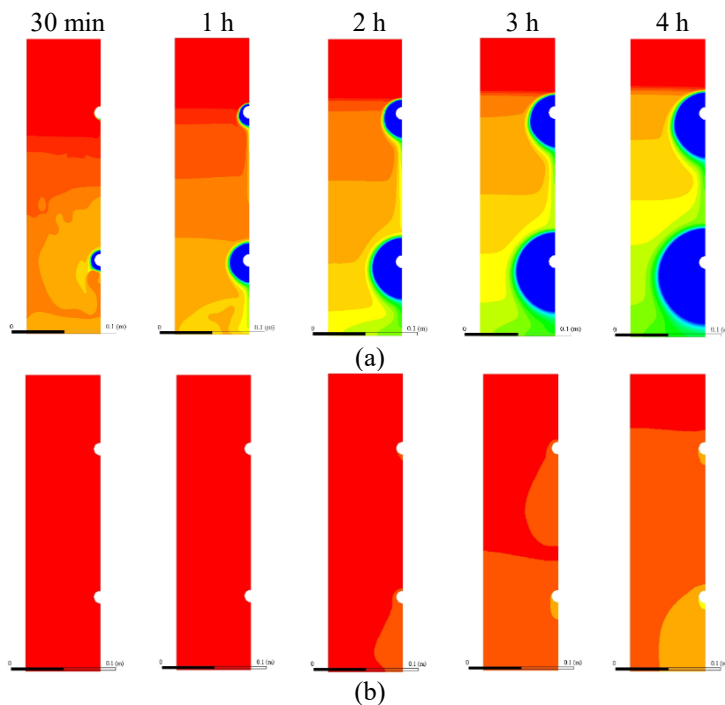


Figure 9: Liquid fraction contours for solidification process (heating rate of 125 W) at different elapsed times. (a) Solar salt; and (b) Metallic PCM.

Fig. 10 shows the liquid fraction versus the time during the solidification process for the considered PCMs at two different heating rates. The metallic PCM solidification process is almost linear as in the melting process. Fig. 11 shows the average temperature versus the

time during the solidification process and the phase change process for the metallic PCM can be clearly identified as it was during the melting process. For solar salt the solidification process has predominantly a linear tendency, however the solidification rate changes at the instance when only 30% of volume is filled by the liquid fraction. The average temperature in the LHTES with solar salt decreases continuously along of the solidification process.

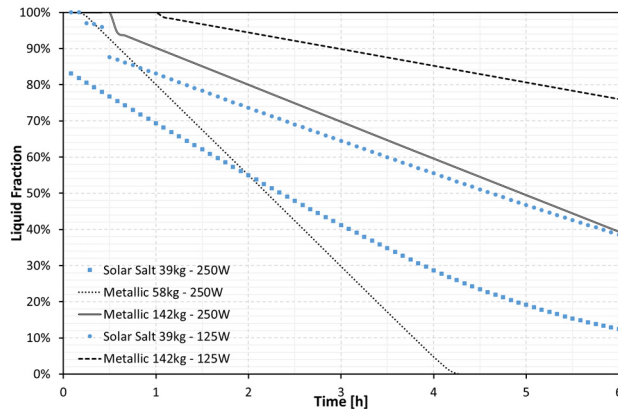


Figure 10: Liquid fraction versus time during solidification process.

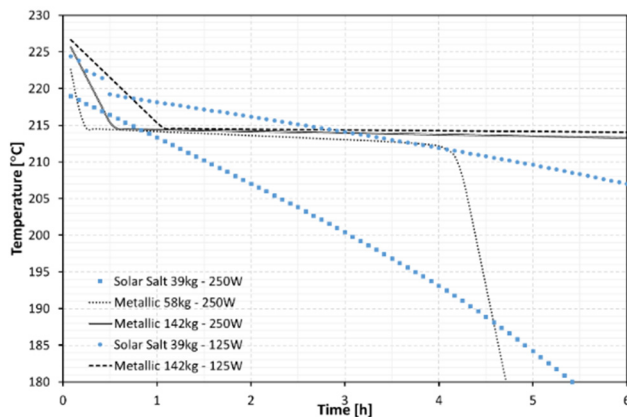


Figure 11: Average temperature versus time during solidification process.

Table 5 shows the numerical results for the solidification times and average temperature for both PCMs studied. The times are the elapsed time from the beginning of the simulation until the volume occupied by the liquid fraction is 10% of the total volume. It can be observed that for the metallic PCMs the average temperature in the LHTES is practically the “solidus” temperature in all cases. However, for solar salt, the temperatures present a significant deviation from the “solidus” temperature. It can be also seen that for the metallic PCM the final solidification time is practically the same as the melting time. Results show that the metallic LHTES, designed for 1 kWh capacity can be discharged in approximately 4 hour

time providing heat at the rate of 0.25 kW. However, the solar salt LHTES designed for 1 kWh capacity requires approximated 8 hour time to be discharged for the same conditions, and this represents a significant deviation from the initial requirement. Considering the final average temperature of solar salt after discharging, the LHTES will require additional energy and time to be recharged.

Table 5: Numerical results for solidification process (10% liquid fraction).

PCM/LHTES capacity	Total HP power (W)	Solidification time (h)	Average temperature (°C)
Solar salt/1kWh	250	6.7	166
Metallic/1 kWh	250	3.8	213
Metallic/2.5 kWh	250	8.9	213
Solar salt/1kWh	125	11.1	187
Metallic/2.5 kWh	125	20.3	213

The numerical results indicate that there are significant differences in the performance of the LHTES using solar salt or metallic PCMs. The differences are in terms of discharging and charging times, average temperatures, melting and solidification processes. Moreover, the design of the LHTES also presents significant differences in terms of dimensions, weight, shape, simplicity and cost. The design of the solar salt LHTES is more complex because the numerical analysis is required in order to evaluate the best arrangements and configuration of heat transfer devices inside the unit. Furthermore, the use of thermal conductivity enhancement methods is necessary in order to fulfil charging and discharging time requirements, affecting the final weight and cost of the LHTES.

#### 4 CONCLUSIONS

In the present work, the melting and solidification processes of two medium temperature PCMs, namely solar salt and metal alloys, were studied in a rectangular LHTES cell. The melting process in the case of the metallic PCM is dominated by the thermal conduction, and in the case of solar salt at the beginning of the process by the natural convection and then, for the thermal conductivity. Therefore, the design of the metallic LHTES with a constant heat flux type heater/sink can be carried out with relatively simple analytical calculations, which also provide good estimation of the charging and discharging times. The design of the solar salt LHTES is more demanding because the multidimensional numerical analysis might be required in order to determine the best arrangement and configuration of heat transfer devices. The results shown superior performance of the metallic PCMs in terms of controlling the charging and discharging rates. However, the applications of this kind of PCMs are limited by the increment in weight and cost.

#### ACKNOWLEDGEMENTS

This project has received funding from the European Union's Horizon 2020 Research and Innovation Programme under Marie Skłodowska-Curie grant agreement No. 705944 (THERMOSTALL). This study is also a part of the "Innova MicroSolar" Project, funded by the European Union's Horizon 2020 Research and Innovation Programme under the grant agreement No 723596.



## REFERENCES

- [1] Lin, Y., Jia, Y., Alva, G. & Fang, G., Review on thermal conductivity enhancement, thermal properties and applications of phase change materials in thermal energy storage. *Renewable and Sustainable Energy Reviews*, **82**, pp. 2730–2742, 2018.
- [2] Yang, X.-H., Tan, S.-C., He, Z.-Z. & Liu, J., Finned heat pipe assisted low melting point metal PCM heat sink against extremely high power thermal shock. *Energy Conversion and Management*, **160**, pp. 467–476, 2018.
- [3] Birchenall, C.E.T., Thermal storage in metals. *Sharing the Sun: Solar Technology in the Seventies, Proceedings of the Joint Conference*, Winnipeg, Canada and Cape Canaveral, Florida, International Solar Energy Society, **8**(A77-48910 23-44), pp. 138–154, 1976.
- [4] Mahkamov, K. et al., Development of a small solar thermal power plant for heat and power supply to domestic and small business building. *ASME Power & Energy*, Lake Buena Vista, Florida, USA, p. 10, 2018.
- [5] Hoshi, A., Mills, D.R., Bittar, A. & Saitoh, T.S., Screening of high melting point phase change materials (PCM) in solar thermal concentrating technology based on CLFR. *Solar Energy*, **79**(3), pp. 332–339, 2005.
- [6] Jankowski, N.R. & McCluskey, F.P., A review of phase change materials for vehicle component thermal buffering. *Applied Energy*, **113**, pp. 1525–1561, 2014.
- [7] Kenisarin, M. & Mahkamov, K., Salt hydrates as latent heat storage materials: Thermophysical properties and costs. *Solar Energy Materials and Solar Cells*, **145**(3), pp. 255–286, 2016.
- [8] Costa, S.C. et al., Experimental and numerical study on melting of solar salt in a finned metallic container. Presented at *ASME 2018 International Mechanical Engineering Congress and Exposition*, American Society of Mechanical Engineers, 2018.
- [9] Bauer, T., Pflieger, N., Breidenbach, N., Eck, M., Laing, D. & Kaesche, S., Material aspects of solar salt for sensible heat storage. *Applied Energy*, **111**, pp. 1114–1119, 2013.
- [10] Mitra, S.S., Viscosity and density of liquid metals. *Physica*, **24**(1–5), pp. 155–156, 1958.
- [11] Yagodin, D., Sidorov, V., Janickovic, D. & Svec, P., Density studies of liquid alloys SnAg and SnZn with near eutectic compositions. *Journal of Non-Crystalline Solids*, **358**(21), pp. 2935–2937, 2012.
- [12] Dobosz, A. & Gancarz, T., Reference data for the density, viscosity, and surface tension of liquid Al–Zn, Ag–Sn, Bi–Sn, Cu–Sn, and Sn–Zn eutectic alloys. *Journal of Physical and Chemical Reference Data*, **47**(1), 2018.
- [13] Meydaneri, F., Saat, B. & Ozdemir, M., Thermal, electrical, microstructure and microhardness properties of the eutectic Sn-3.5wt.%Ag alloy, 2013.
- [14] Ocak, Y., Aksöz, S., Maraşlı, N. & Keşlioğlu, K., Thermal conductivity and interfacial energies of solid Sn solution in the Sn–Ag–In ternary alloy. *Chemical Physics Letters*, **496**(4–6), pp. 263–269, 2010.
- [15] Çadırlı, E., Şahin, M., Kayalı, R., Arı, M. & Durmuş, S., Dependence of electrical and thermal conductivity on temperature in directionally solidified Sn–3.5 wt.% Ag eutectic alloy. *Journal of Materials Science: Materials in Electronics*, **22**(11), pp. 1709–1714, 2011.
- [16] Tiari, S., Qiu, S. & Mahdavi, M., Discharging process of a finned heat pipe-assisted thermal energy storage system with high temperature phase change material. *Energy Conversion and Management*, **118**, pp. 426–437, 2016.



- [17] Tiari, S., Qiu, S. & Mahdavi, M., Numerical study of finned heat pipe-assisted thermal energy storage system with high temperature phase change material. *Energy Conversion and Management*, **89**, pp. 833–842, 2015.
- [18] Lohrasbi, S., Miry, S.Z., Gorji-Bandpy, M. & Ganji, D.D., Performance enhancement of finned heat pipe assisted latent heat thermal energy storage system in the presence of nano-enhanced H<sub>2</sub>O as phase change material. *International Journal of Hydrogen Energy*, **42**(10), pp. 6526–6546, 2017.
- [19] Guo, C. & Zhang, W., Numerical simulation and parametric study on new type of high temperature latent heat thermal energy storage system. *Energy Conversion and Management*, **49**(5), pp. 919–927, 2008.
- [20] Cengel, Y.A., *Heat Transfer*, 2nd ed., McGraw-Hill: London, 2007.

